

Chapter 2

Mosaic Cameras

Version 1.1, May 2009

In This Chapter...

Instrument Overview	2-1
Data Products	2-7
Calibration	2-15
Sources of Error	2-27
References & Further Information	2-30

The Mosaic cameras have been in operation at NOAO since the late 1990s, and a good deal of technical literature exists on the instrument design, operation, and performance. The material presented here is drawn primarily from the *NOAO CCD Mosaic Imager User Manual* (Schweiker & Jannuzi 2004), and from the *NOAO Deep Wide-Field Survey Mosaic Data Reductions* notes by Jannuzi, Claver, & Valdes (2003). Interested users should consult these authoritative documents for details of the instrument configuration and operation. Additional resources are cited throughout this chapter and are listed along with other background material in the last section.

2.1 INSTRUMENT OVERVIEW

The Mosaic cameras are among the most heavily used instruments offered by NOAO, as measured both by number of nights awarded to principal investigator (PI) programs, and by the volume of data in the NOAO Science Archive. There are actually two Mosaic cameras: **Mosaic-1** is used on both the Mayall 4-m and the WIYN 0.9-m telescopes on Kitt Peak, and **Mosaic-2** is used on the Blanco 4-m telescope at Cerro Tololo. This chapter will cover all usages of both cameras; differences in the instrument design, usage, or other technical details that affect the data will be called out.

2.1.1 Instrument Capabilities & Design

The Mosaic cameras are optical/near-IR imagers with a wide field of view (FoV) and a large focal plane array (FPA) containing a total of 8096×8096 pixels. A schematic of the instrument is shown in Figure 2.1. The detectors reach peak quantum efficiency (QE) above 85% at $\sim 6500 \text{ \AA}$, but have useful sensitivity from the atmospheric cut-off near 3200 \AA to $\sim 1 \text{ \mu m}$. Both KPNO and CTIO have a large number of filters¹ that are designed to be used with these cameras, up to 14 of which can be held in the *filter track* at one time. The filter sets include standard broad bandpasses, such as Harris *UBV* and Cousins *R*, SDSS *g'r'i'z'*, narrowband filters near $H\alpha$, $[\text{O III}] \lambda 5007$, and various other nebular emission lines. Other filters, including filters provided by PIs for their observing programs, have been used occasionally.

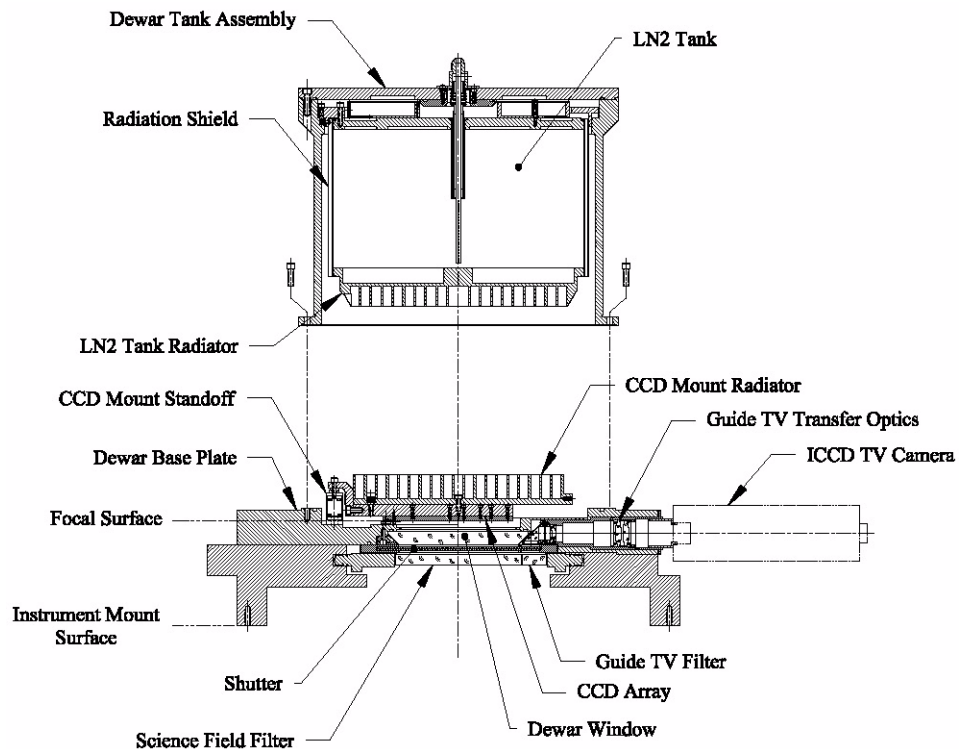


FIGURE 2.1: Cross-section view of the Mosaic dewar, also showing the arrangement of the CCD array and the filter. Light enters from below in this diagram and passes through the corrector optics (not shown).

The details of the observing configurations for the Mosaic cameras are given in Table 2.1. The cameras are mounted at the Prime focal station of the 4-m telescopes, and at the Cassegrain focus of the 0.9-m, with converging beams as indicated in the Table. The detectors sample the delivered point spread function

1. Filter properties can be viewed at <http://www.noao.edu/kpno/mosaic/filters/filters.html>.

(PSF) very well; image quality is seeing-limited at all wavelengths. The image quality at the 4-m telescopes is good, with little (<10%) focus gradient or PSF variation across the field of view. The pixel scale is slightly variable from the center to the edge of the field of view due to pincushion distortions. The image quality at the 0.9-m telescope is not as good: there is a small focus gradient across the FoV, resulting in degraded images near the corners of the field. Also, the corners of the field are slightly vignetted (~5–10%) by the internal telescope baffle. The image scale at the 0.9-m is relatively constant across the FoV.

TABLE 2.1: Mosaic Observing Configurations

	KPNO 4-m	CTIO 4-m	WIYN 0.9-m
Field of view	36' × 36'	36' × 36'	59' × 59'
Pixel scale @center/edge of FoV (arcsec/unbinned pixel)	0.261 / 0.245	0.261 / 0.245	0.425 / 0.420
ADC ^a usage	Recommended	Recommended	N/A
Telescope focal ratio	f3.1	f2.9	f7.9

a. Atmospheric Dispersion Corrector.

An atmospheric dispersion corrector (ADC) is available on the 4-m telescopes for the Mosaic cameras (see Jacoby, et al. 1998 for details). The effect of atmospheric dispersion is greatest for very wide filters, and especially in the blue (stretching a stellar image by 0.9 arcsec in the *U* filter at a zenith distance of 60°, or 2 airmasses). Because of the wide FoV of the Mosaic cameras, differential atmospheric refraction within the FoV is noticeable even at the zenith.



Note that the ADC is used at the discretion of the observer, so that subsequent users of the 4-m Mosaic data will need to examine the value of the ADC header keyword to determine if any given image was obtained with the ADC. Since no ADC is available at the WIYN 0.9-m telescope, images obtained there at high airmass will suffer significant image degradation.

The shutter for the Mosaic cameras consists of a pair of opposing sliding blades, which serves to regulate the exposure time. The motion of the shutter blades is along columns, and the time-of-flight is approximately 23 ms. The accuracy of the shutter timing is good, but not perfect: one experiment showed that a 1 s exposure illuminated the FPA for 0.97 s at the top of the array, and 0.96 s at the bottom. A shutter shading correction is in principle possible, but most Mosaic science data are obtained with exposures greatly exceeding 1 s so that the correction would be negligible.

Focal Plane

The focal plane of the Mosaic cameras is populated with an array of eight SITE CCD detectors, arranged in a 4×2 mosaic, as shown in Figure 2.2. Each of the thinned CCD detectors has two amplifiers to provide the capability of reading the arrays using either or both amplifiers. The Mosaic-2 camera is generally operated with all 16 amplifiers. The Mosaic-1 camera does not have working dual amplifiers on all CCDs, and so can only be used with one amplifier per CCD. All the detectors have very few cosmetic defects.

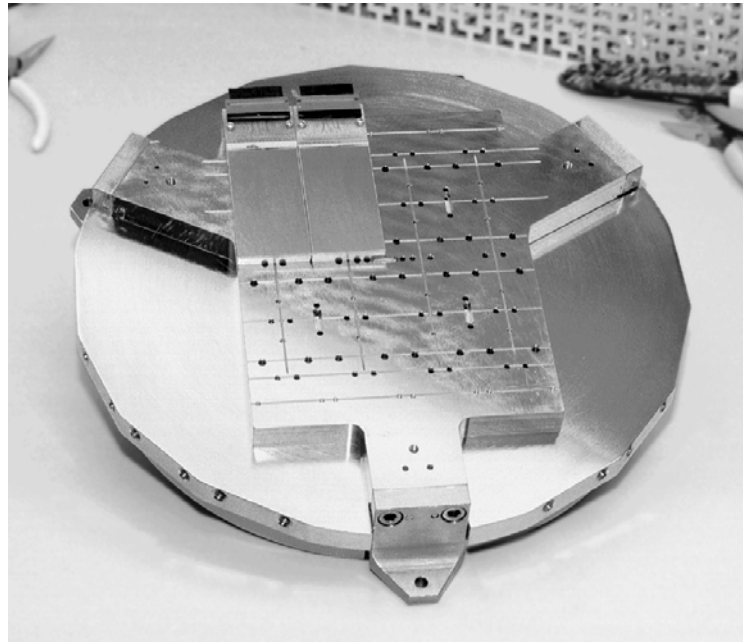


FIGURE 2.2: Mounting for the Mosaic-1 detectors, showing two of the eight 2048 x 4096 pixel CCD arrays in position.

The detector properties, or ranges of properties, are given in Table 2.2. The linearity is good, but the dynamic range is modest by modern standards and varies from detector to detector. The charge transfer efficiency (CTE) when the detectors were first installed was excellent (0.999995 or better), and is not believed to have degraded significantly since then. The pixels may be binned at read-out by integral factors. Observers have selected this option with some regularity to reduce the read-out time (e.g., for observations of variable phenomena or moving targets that require a rapid cadence), or to reduce the read noise per binned pixel (compared to post-read down-sampling). The penalty, of course, is the possibility of under-sampled images and reduced spatial resolution, depending upon the delivered image quality at the time of the observations. Finally, the QE varies somewhat from detector to detector, both on average and as a function of wavelength. (See the Mosaic instrument manuals for details.) Therefore the

transformation from instrumental magnitudes to standard systems depends upon the detector. See “Photometric Calibration” on page 2-21 and “Photometry” on page 2-28.

TABLE 2.2: CCD Array Characteristics

Array Dimensions	
Axis 1:	2048 pixels
Axis 2:	4096 pixels
Pixel Size	15 μm square
Binning factors ^a	1, 2, 3, 4
Gain	1.8 to 3.3 e^-/ADU
Read noise	5.0 to 9.0 e^-
Max. linear count	21,000 to 45,000 e^-
CCD Gaps	
in rows:	50 unbinned pixels
in columns:	35 unbinned pixels
Exposure overheads ^b	
binned 1 \times 1	2:34 (min:sec)
binned 2 \times 2	1:06 (min:sec)

a. Configurable by observer, independently for each image axis.

b. Times dominated by detector read-out, assuming a single amplifier.

Figure 2.3 shows the arrangement of the FPA on the sky, which differs between hemispheres, using the same nomenclature as is found in the science data extension headers. Note that the raw image array coordinates are remapped from the detector coordinates, such that the origin is always in the lower-left corner when oriented as in the figure. For reduced data, the images are transposed so that North is up and East is to the left.

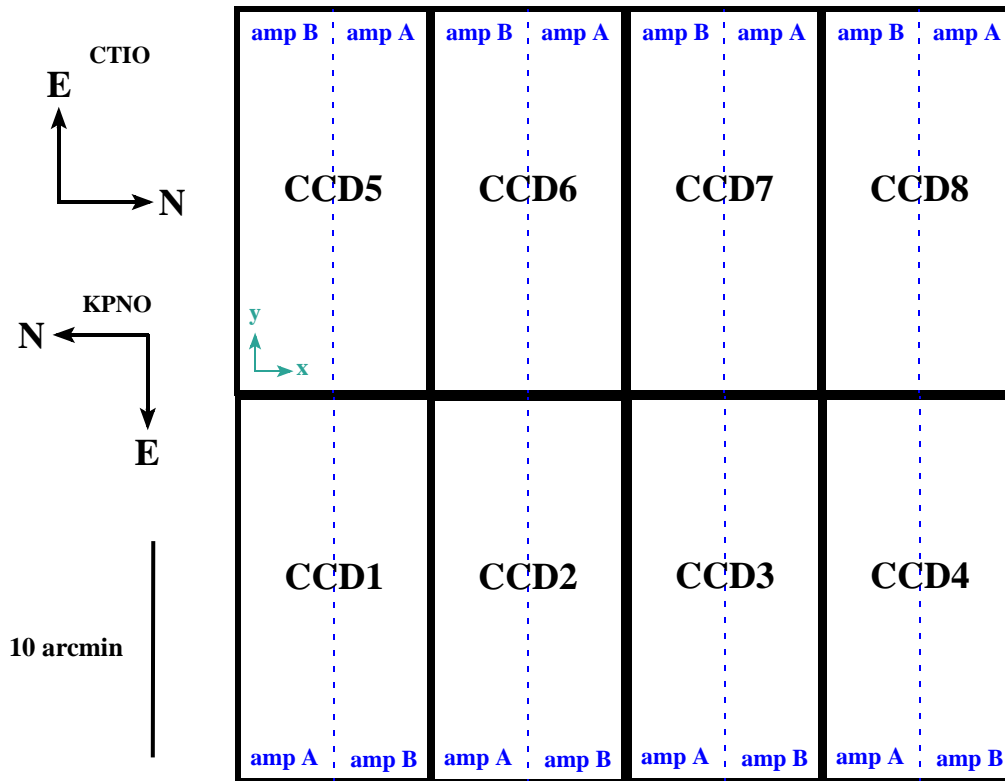


FIGURE 2.3: Orientations on the sky and spatial footprint of the FPA for both Mosaic cameras, with CCD detector designations indicated. Two amplifiers on each chip may be used for parallel read-out (CTIO Mosaic-2 only) over areas bounded by dotted lines. Image coordinate axes are also indicated (small arrows); pixel coordinate origin is in the lower-left corner of each detector array (or sub-array).

Operations

Most data obtained with the Mosaic cameras have a binning of 1×1 or 2×2 pixels. Many observers obtained multiple exposures of their fields using the same filter in order to reject cosmic rays; often this was combined with a sequence of small spatial dithers in order to observe in the gaps between the CCDs in the FPA, and to enable the construction of continuous regions of sky free of gaps and detector artifacts. A few observing programs construct sequences of (slightly) overlapping images to map large regions of sky from the component tiles. Finally, most observing programs obtain calibration frames, such as bias (zero) frames and dome flats, in order to facilitate calibration. See “Calibration” on page 2-15 for a detailed discussion of how the calibration frames are used in the data reduction process.

2.2 DATA PRODUCTS

This section describes the content and format of the various data products that are produced for the Mosaic cameras. Most of the products are generated during the course of calibration processing, the details of which are discussed in the next subsection. The data products can be distinguished by the combination of the PROCTYPE, PRODTYPE, and OBSTYPE keywords in the primary header; the possible values are summarized in Table 2.3. The processing level (see Table 1.2, “Levels of Data Processing,” on page 1-4) at which the product is generated is listed in column 5 (Proc. Level).

TABLE 2.3: Data Product Content Type

PROCTYPE	PRODTYPE	OBSTYPE	Extensions	Proc. Level	Description
Raw	image	object zero dark dome flat	IMAGE * N _{ext}	1	Raw data as obtained at the telescope, with additional metadata included in the header. Note: OBSTYPE value unreliable in raw data.
InstCal	image	object	IMAGE * N _{ext}	2	Calibrated, single-frame reduced image with instrument signature removed, WCS and rough photometric calibrations applied
InstCal	dqmask	object	BINTABLE * N _{ext}	2	Data quality mask for InstCal
InstCal	png	object	FOREIGN*2	2	Down-sampled preview for InstCal
Resampled	image	object	[none]	2	Calibrated, re-projected image
Resampled	dqmask	object	BINTABLE	2	Data quality mask for resampled image
Resampled	png	object	FOREIGN*2	2	Preview for resampled image
Stack	image	object	[primary]	3	Stack of 2 or more overlapping images
Stack	dqmask	object	BINTABLE	3	Data quality mask for stacked image
Stack	expmap	object	BINTABLE	3	Exposure map for stacked image
Stack	png	object	FOREIGN*2	3	Preview for stacked image
MasterCal	image	zero	IMAGE * N _{ext}	2	Bias structure image template
MasterCal	png	zero	FOREIGN*2	2	Preview for bias structure
MasterCal	image	dome flat	IMAGE * N _{ext}	2	Dome flat-field template image
MasterCal	png	dome flat	FOREIGN*2	2	Preview for dome flat
MasterCal	image	sky flat	IMAGE * N _{ext}	2	Sky delta-flat-field image
MasterCal	png	sky flat	FOREIGN*2	2	Preview for sky flat
MasterCal	image	pupil	IMAGE * N _{ext}	2	Pupil ghost template image; generated only for Mosaic-1 data obtained at KPNO
MasterCal	png	pupil	FOREIGN*2	2	Preview for pupil ghost template
MasterCal	image	fringe	IMAGE * N _{ext}	2	Fringe pattern template image
MasterCal	png	fringe	FOREIGN*2	2	Preview for fringe pattern

2.2.1 Image Formats

The image data from the Mosaic cameras is stored either in FITS multi-extension files (MEFs), the general structure of which was described in Chapter 1, or, for some reduced data, in simple FITS files with no extensions. Although most images are stored in extensions, the detailed arrangement of the image portions among the extensions differs depending upon whether the data are raw (unprocessed) or reduced, and upon the operational practice for each Mosaic camera.

Raw Data

Raw data from the MOSAIC cameras consists of 16-bit unsigned integers, and includes virtual over-scan along each row at the beginning (pre-scan: 24 pixels) and end (over-scan: 48 or 64 pixels) of the CCD read-outs, which is stored with the image pixels as shown in Figure 2.4. Note that the coordinate origin for all images is in the lower-left corner of the read-out section (for the convenience of image display), rather than at the location of the read-out amplifier. While each detector in both Mosaic cameras has two read-out amplifiers, in practice only the Mosaic-2 camera uses both amplifiers in parallel to read both halves of the arrays simultaneously. The output from each amplifier (including the over-scan regions) is stored in a separate image extension in the FITS MEF file (see Chapter 1); thus, there are as many image extensions in the raw science file as the total number of amplifiers used to read out all detectors in the focal plane. The size and location of the photo-active regions and the over-scan are given in Table 2.4. Note that the size of the region used for determining the bias level is smaller than the size of the over-scan region, and that the pre-scan area is not used to determine the bias level.

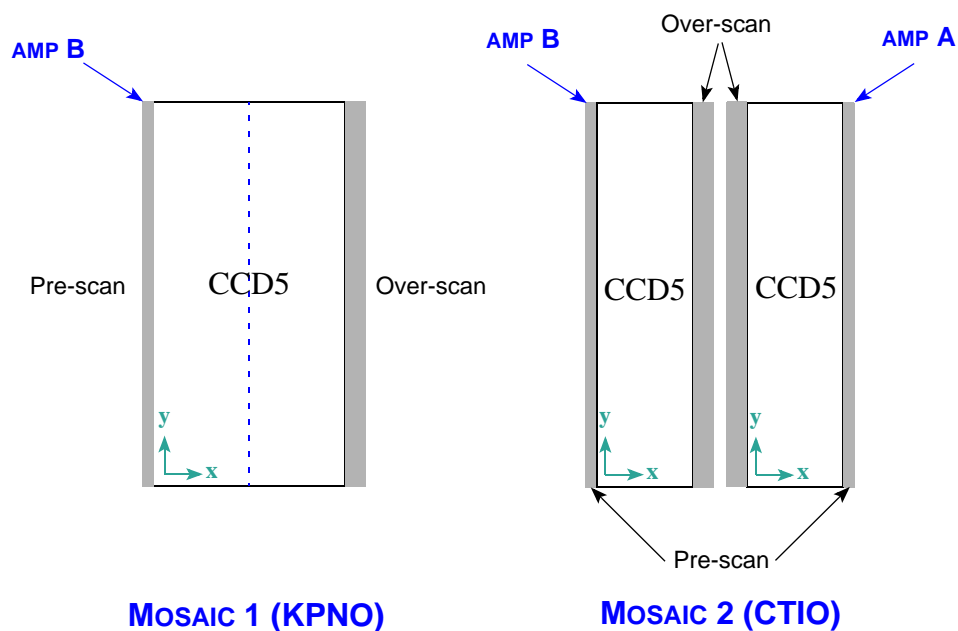


FIGURE 2.4: Schematic of the image arrays just after read-out for detector 5 of the Mosaic camera used at Kitt Peak (*left*) and Cerro Tololo (*right*). Virtual over-scan regions are indicated in grey, but are expanded horizontally by a factor of 4 for clarity. Amplifier locations are indicated, as is the orientation and approximate origin of the pixel coordinate axes (small arrows).

TABLE 2.4: Raw Data and Over-scan Regions

Raster Dimensions	Detectors	Amp	Photo-Active Data Section	Bias Section (Columns)
Mosaic-1				
2136 × 4096	1–4	B	[65:2112, 1:4096]	[1:50]
	5–8	B	[25:2072, 1:4096]	[2087:2136]
Mosaic-2				
1112 × 4096	1–4	A	[25:1048, 1:4096]	[1063:1112]
		B	[65:1088, 1:4096]	[1:50]
	5–8	A	[65:1088, 1:4096]	[1:50]
		B	[25:1048, 1:4096]	[1063:1112]

Calibrated Data

The Archive contains data products that are produced with the Mosaic calibration pipeline. The specific calibrated science data products are listed in Table 2.3 on page 2-7 and are described in more detail below. Each image has an associated *data quality mask* (DQM) and a *preview image*, which are described at the end of this subsection. The science images are stored as 16-bit scaled integers, which is a mild form of compression, when the sigma of the sky pixels can be sampled at more than 30:1 with a dynamic range over all non-flagged pixels. That is, the integer digitization has at least 30 values within 1-sigma of the sky distribution, and the 32K values span all good (i.e., non-flagged) pixel values in the calibrated data. If these conditions cannot be met, then the images are stored as 32-bit floating-point values.

InstCal. These images have been processed to remove instrumental signature, and have been astrometrically and photometrically calibrated (see “Calibration” on page 2-15), although there are some cases where the calibration can fail (see “Sources of Error” on page 2-27). The data are organized almost identically to that for the raw science data, except for the following:

- The over-scan regions have been trimmed from the image arrays.
- Image portions for a given detector that were read by different amplifiers have been joined. Thus, even science files from the Mosaic-2 camera contain 8 image extensions, one for each detector.
- The resulting images in each extension are all 2048×4096 pixels.

Resampled. These images are the result of geometrically rectifying InstCal images, where each array has been re-projected to a common tangent-point on the sky, with pixels aligned to a common grid with uniform scale. The pixels have been transposed, so that when displayed, images will appear with North “up” (i.e., declination increases along Axis 2) and East “left” (i.e., Right Ascension decreases along Axis 1). The images are stored in the primary header-data unit within the file. The tangent-point is selected from a grid with roughly 1° steps in RA, and exactly 1° in Dec. The aim is to maximize the probability that exposures from different nights and processing runs may be combined without requiring further interpolation. Within a single night, all overlapping exposures, such as from dither sequences or serendipitous overlapping pointings, are assigned a common tangent point even if some elements of a dither would have been assigned to different grid points when considered independently. The resampled images are approximately 8526×8642 pixels; the actual size depends on the degree of differential atmospheric refraction and the WCS tangent point selected for a particular image.

Stacked. If two or more observations of a given target are obtained on the same night using the same filter and have a sufficient degree of spatial overlap, these images are combined using an average with outlier rejection to remove

detector blemishes, gaps between the detectors, and artifacts such as image persistence and cosmic rays. The result is a union of the spatial footprints of the stack, which is stored in a simple FITS image (i.e., not in image extensions), with nearly the same pixel scale as the raw images. In general, these images will be larger—sometimes very much larger—than the resampled images because the area of the sky that is mapped can be significantly larger than the instrument FoV.



The exposure duration for stacked images, as recorded in the `EXPTIME` keyword, refers to the sum of all exposure durations of all images used to create the stack. The exposure depth and noise properties of a stack of dithered images is a discontinuous and possibly complicated function of position in the image. Use the exposure map to track the detailed exposure depth at the pixel level.

Master Calibration. Reference files are created during the course of pipeline processing, such as bias structure, flat-fields, etc. These files are used in pipeline processing to remove instrumental signatures from the science data. (See “Calibration Reference Files” on page 2-23.) These reference files are 32-bit floating-point images, stored as MEF files with as many extensions as the corresponding raw images.

Concomitant Data. All reduced images are accompanied by data quality masks (DQM); stacked images are accompanied in addition by exposure maps. The DQMs and exposure maps are logically images, but they are stored in compressed form as FITS binary tables, with one table per extension in the science image. Some utilities (such as the IRAF `XImtool`) can display and work with these files directly, but other utilities may require that the files be translated to FITS images before they can be used. The pixel values in the DQMs are non-zero when affected by detector pathologies and image artifacts such as bleed trails, saturation, and cosmic rays; the values are zero otherwise. Table 2.5 lists mask values that are applicable to *nonstacked* images.

TABLE 2.5: Data Quality Mask Values

Value	Meaning
0	No problem
1, 6	Bad/compromised pixel identified in static DQM; generally indicates known detector blemishes
2	[Not used]
3	[Not used]
4	Saturated (plus padding)

TABLE 2.5: Data Quality Mask Values (Continued)

Value	Meaning
5	Bleed trail (plus padding); indicates possibly compromised pixels
7, 8	Transient artifacts (includes cosmic rays)

Most *stacked* images are created from dithered frames, so that most of the pathologies affecting single frames will not be applicable. DQMs for stacked images have the following values: “1” for areas of the re-projected image with no data, “2” for areas with no data *after rejection*, and zero otherwise.

The exposure maps are images whose values are the cumulative exposure duration at each pixel, which can be a complicated function of position. The value of the `EXPTIME` keyword in a stacked image is the sum of the exposure durations for all images that contributed to the stack.

Ancillary Files. The preview images are down-sampled versions of the files they accompany and are stored in Portable Network Graphics² (PNG) format. There are two samplings for each file, which are intended mainly for quick display of the results of pipeline processing on Web pages. Note that these files have been embedded in FITS files as extensions of type `FOREIGN` so that most users will need to extract them with some tool before viewing.

2.2.2 Header Keywords

A wide variety of metadata are recorded in the headers of the science frames. Users should review these headers (and the extension headers) to familiarize themselves with the content. The more critical metadata are described in this subsection. Table 2.6 lists metadata by the keyword name, the header unit in which the keyword will be found (Primary or Extension), the point in the data processing where the keyword is introduced (or where the value is updated), and the meaning of the keyword (or group of keywords, if they are related). Some of the keywords are indexed by image axis, meaning they come in pairs, as indicated by the suffixes *i* and *j*.

2. <http://www.libpng.org/pub/png/>

TABLE 2.6: Important Image Keywords

Keyword Name	HDU	Origin	Meaning
Telescope			
ADC	P	R	Identification of the Atmospheric Dispersion Corrector (ADC)
ADCSTAT	P	R	ADC tracking status
AIRMASS	P	R	Atmospheric pathlength for target at observation start
OBSERVAT	P	R	Observatory that operates this telescope
TELESCOP	P	R	Telescope used to obtain these data
TELDEC	P	R	Declination for the telescope position on the sky in degrees
TELRA	P	R	Right ascension for the telescope position on the sky in hours
Instrument/Detector Configuration			
CCDSUM	E	R	CCD binning factors along Axis1 and Axis2
DETECTOR	E	L2	Detector designation
FILTER	P	R	Filter name/designation
GAIN	E	R, U	Detector effective gain, in e^-/ADU
INSTRUME	P	L2	Instrument name
OGAIN	E	L2	Original detector gain setting for the exposure, in e^-/ADU (same as GAIN for raw images)
Time			
DATE-OBS	P	R	Date and time of observation start
EXPTIME	P	R	Effective exposure duration in seconds
MJD-OBS	P	R	Time of observation start in MJD
TIME-OBS	P	R	Time of observation start
TIMESYS	P	R	The principal time system for all time-related keywords. Always UTC.
World Coordinates			
CDi_j	E	R, U	Transformation matrix from pixel to intermediate world coordinates; CDi_i is the pixel scale for axis i
$CRPIXi$	E	R, U	Location of the reference point along axis i in units of pixels
$CRVALi$	E	R, U	Value of the world coordinate at the reference point for axis i in degrees
$CTYPEi$	E	R	Name of the coordinate represented in axis i
DEC	P	R, U	Declination for the center of the detector FoV in degrees
EQUINOX	E	R	Equinox in years for the celestial coordinate system in which the positions are expressed
$NAXISi$	E	R	Number of pixels along axis i
$PIXCALi$	E	R	Pixel scale along axis i in arcsec/pixel

TABLE 2.6: Important Image Keywords (Continued)

Keyword Name	HDU	Origin	Meaning
RA	P	R, U	Right ascension for the center of the detector FoV in hours
RADESYS	E	R, U	Name of the reference system in which the world coordinates are expressed
WATi_nnn	E	R, U	IRAF-specific description of the nonlinear portion of the transformation from detector to world coordinates for axis <i>i</i> . This character string contains coefficients for a polynomial; the length of the string is such that it must continue for <i>nnn</i> FITS header records.
Calibration			
BLDPROC	E	L2	Bleed trail processing parameters (bleed threshold & grow radius)
BUNIT	E	L2, L3	Brightness units, normally “electron/s” for calibrated images
MAGZERO	E	L2	Magnitude corresponding to one count in the image
OBSTYPE	P	R, U	Type of target observed (see Table 2.3 on page 2-7)
PHOTBW	P	L2	RMS width of bandpass (Å)
PHOTCLAM	P	L2	Central wavelength of bandpass (Å)
PHOTDPTH	P	L2	Photometric depth of the exposure. (See “Photometric Calibration” on page 2-21.)
PHOTFWHM	P	L2	FWHM of bandpass (Å), i.e., width measured at 50% of peak transmission
PIPELINE	P	L2, U	Pipeline name
PLVER	P	L2, U	Pipeline version identifier
PROCTYPE	P	L2, U	Product type (see Table 2.3 on page 2-7)
PRODTYPE	P	L2, U	Product data description (image mask expmap)
SATPROC	E	L2	Saturation processing parameters (saturation threshold & grow radius)
SEEING	P	L2	Average FWHM of point sources in arcseconds
SKYBG	P	L2	Brightness level of background averaged over all CCDs in ADU
SKYBG1	E	L2	Brightness level of background in single CCD in ADU
SKYNOISE	P	L2	RMS noise in the background level in ADU

2.2.3 Environmental Data

At present no environmental data are accessible from the Archive, although data from all-sky cameras and seeing monitors is planned. A terse summary of sky conditions at CTIO³ and at KPNO⁴ are available on the Web.

3. http://www.ctio.noao.edu/site/phot/sky_conditions.php

4. http://www-kpno.kpno.noao.edu/Info/Mtn_Weather/

2.3 CALIBRATION

The current generation of pipeline processing produces Level-2 products, i.e., images where the instrumental signature has been removed and geometric and photometric calibrations have been applied; and Level-3 products, where spatially overlapping images in the same filter (and that have been obtained within the same observing run) have been stacked. The pipeline uses both calibration exposures, such as bias frames and dome flats, as well as portions of science exposures (i.e., areas free of defects, artifacts, and astrophysical objects) to construct the calibration reference files that are used as input to the processing. For simplicity, the subsections below will first describe the processing of the science images once the calibration reference files are available; then the processes for constructing the calibration reference files will be described with the overall flow as context. The actual sequence of processing in the pipeline software differs somewhat in detail, in part to optimize the performance of the parallel processing environment.



The calibration pipeline for Mosaic reductions is very much tuned to maximize the use of exposures within the observing run in which they were obtained. As such, the quality of the data depends to a large degree on the quality of the calibration exposures that were obtained by the observer. However, under some circumstances, the pipeline will attempt to use calibration data from prior observing runs if the separation in time is not too great; the specific rules are described in the following sections.



This pipeline *does not* process Mosaic data that were obtained with the WIYN 0.9-m telescope. This pipeline *only* processes data obtained with a CCD binning of 1×1 (using either 4-m telescope).

2.3.1 Processing Steps

The flow of the science data through the pipeline is shown in Figure 2.5. Each step of the processing, indicated by the boxes in the center of the figure, is described in detail in the following subsections. As explained below, some steps are not performed for data where the correction in question is not needed. Inputs to the processing include the raw science frames, calibration reference files (see “Calibration Reference Files” on page 2-23), and photometric and astrometric catalogs. Outputs include the various reduced science images, plus their associ-

ated mask files (see “Image Formats” on page 2-8). Intermediate products that are produced during the course of pipeline processing, but that are not archived, are not shown. The processing is segregated by night, filter, and further by overlapping observing sequences when deriving stacked frames.

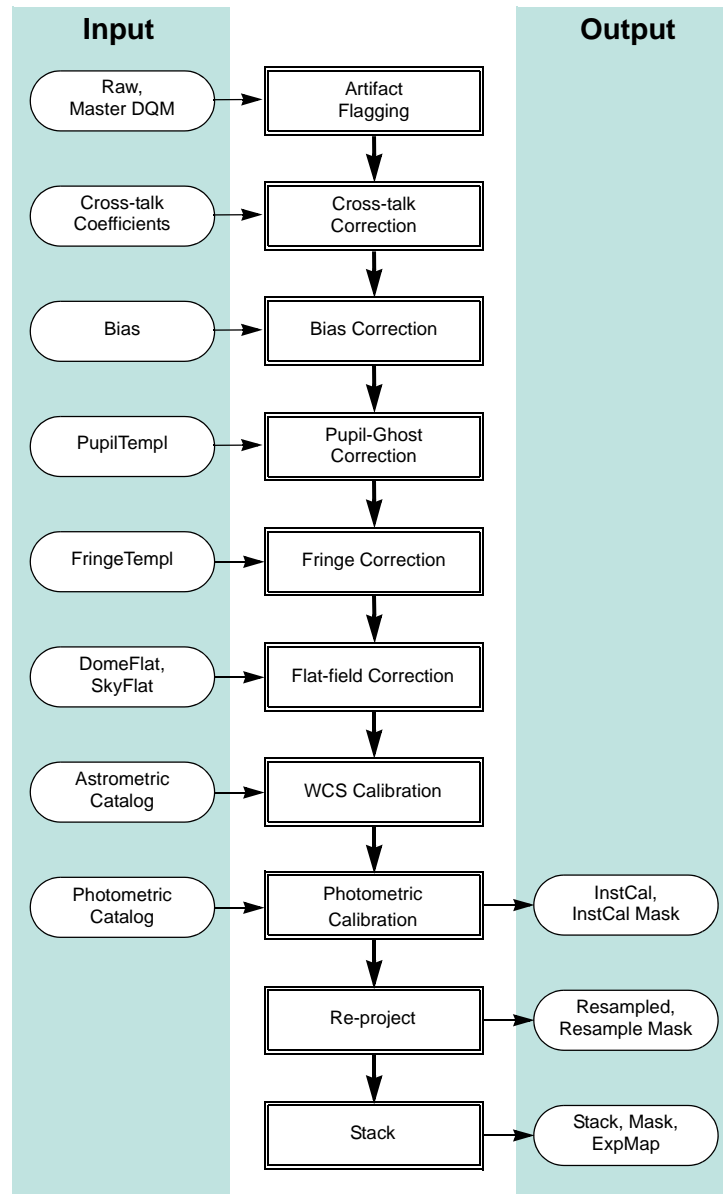


FIGURE 2.5: Flow of data taken with a common filter through pipeline processing and calibration to produce Level-2 and Level-3 data products. Note that pupil ghost correction only applies to Mosaic-1 data from the 4-m telescope. External catalogs, and data products defined in Table 2.3, are shown as inputs or outputs of the processing.

Artifact Flagging

Various image artifacts, including detector defects marked in the Master DQM reference file, are flagged in the DQM for each science image. In addition, pixels with values above the saturation threshold for the parent CCD are flagged at the beginning of the processing. Further artifact flagging occurs later in the processing, including *transients* (e.g., moving objects and cosmic rays) which are detected during the final image stack. Note that the regions flagged using the saturation and bleed trail thresholds are grown by up to a few adjacent pixels to minimize the risk of compromised data near artifacts. The final data quality mask for each InstCal image indicates all detected artifacts noted above; these values are propagated to the Resampled images, which generally increases the number of affected pixels to include areas adjacent to the pixels in the original geometry. All flagged pixels are excluded from contributing to the final, *stacked* image; if this process results in areas with no data, such pixels are so flagged (see “Concomitant Data” on page 2-11 for details).



Note that all pixels in calibrated science frames (InstCal, Resampled, and Stacked) that are flagged in the DQM with a value other than zero will be interpolated over. The 1-dimensional linear interpolation is performed along the shortest dimension of the region over which to interpolate. This process is intended to avoid introducing “ringing” artifacts during the down-stream resampling of the images, as well as to mitigate scaling problems when using image display software. The affected pixels retain their flags in the DQM, however.

Cross-Talk Correction

A small but significant amount of *cross-talk* occurs between the readout electronics of pairs of CCDs in the FPA. The effect is to introduce a small fraction of the signal from one CCD into the signal chain of the CCD that shares the same electronics box, such that “ghosts” of bright objects appear in the paired CCD. This is an additive effect of ~0.1%, and is most noticeable in objects that are at or near saturation. The proportionality coefficients differ from one electronics box to another, but are relatively stable over time unless significant maintenance has been performed on the instrument. The processing pipeline applies pre-calibrated proportionality coefficients and subtracts the cross-talk signature from the images.

Bias Correction

This correction is applied to remove the (additive) electronic bias that is present in the signal chain. The bias is, for the most part, composed of a constant pedestal, but it has structure that is related to the electronic stability of the bias during read-out of the detector. The processing pipeline removes the bias contribution in a two-step process. In the first step, the post-scan region (see Table 2.4 on page 2-9) is averaged along the serial direction, and this average value for each image line is subtracted. The virtual over-scan regions (i.e., the pre-scan and the post-scan: see Figure 2.4 on page 2-9) are then removed from the image. In the second step, the master bias image is subtracted from each science image to remove higher-order structure.

Following the bias correction, the pixels are scaled by the gain factor for the appropriate CCD and normalized to unit exposure time. The brightness units, as expressed in the value of the BUNIT keyword, are electrons s^{-1} (or equivalently, detected photons s^{-1}) for calibrated images.

Dark Correction

The dark current, i.e., the signal introduced by thermal electrons in the detector with the instrument shutter closed, is extremely low for the Mosaic CCDs, so **no dark correction is presently applied in the processing pipeline**. Were a dark correction to be applied, it would occur after bias correction and would be applied by subtracting a dark master frame from the science frames, after scaling by the ratio of the exposure times.

Pupil Ghost Correction

The pupil ghost is an artifact that is evident in data from the Mosaic-1 camera when used at the 4-m telescope. The artifact is caused by light that reflects off the filter, off the back surface of the corrector, and returns through the filters to the detector. For Mosaic-1, the effect is evident in raw data as an image of the telescope pupil near the intersection of detectors 2, 3, 6, and 7 (see Figure 2.6 on page 2-20). The amplitude of the effect is greatest where the coating of the corrector is least effective (in the extremes of red and blue), particularly in the U , I , and z bands, and in narrowband filters of similar wavelength. The pupil ghost template is scaled to the pattern in the science frame and subtracted.



The pupil ghost correction is only applied to data obtained with the Mosaic-1 camera on the 4-m telescope on Kitt Peak, and only for exposures taken through broadband or narrowband filters with central wavelengths near *U*, *B*, and *I*. No pupil ghost is evident in Mosaic-1 data when used at the WIYN 0.9-m telescope, or in Mosaic-2 data on the CTIO 4-m telescope.

Fringe Pattern Correction

A fringe pattern is evident in data from both Mosaic cameras at certain (mostly red) wavelengths. The pattern occurs because of interference between the incident, nearly monochromatic light from night sky emission lines (from both air glow and reflected city lights) and light that is reflected internally between layers of the CCD substrate. The details of the fringe pattern depend mostly upon the spatial variation in thickness of the top layer in the substrate, but also depend upon a number of other factors including the wavelength(s) of the incident emission lines, the composition of the substrate, the temperature of the CCD, and the focal ratio of the incident beam. (See Walsh, Pirzkal & Pasquali, 2002 for a useful discussion of this phenomenon in the ACS camera on the Hubble Space Telescope.) The amplitude of the fringe pattern background varies with time and telescope pointing. Since the amplitude of the fringes can be large compared to the mean sky background, it is important to remove it where possible. An example of fringing over a portion of an image can be seen in Figure 2.6. To remove the effect, the fringe template is scaled to the science image and subtracted.



The fringe correction is only applied to exposures taken through narrowband filters, or through broadband filters with central wavelengths greater than 6290 Å.

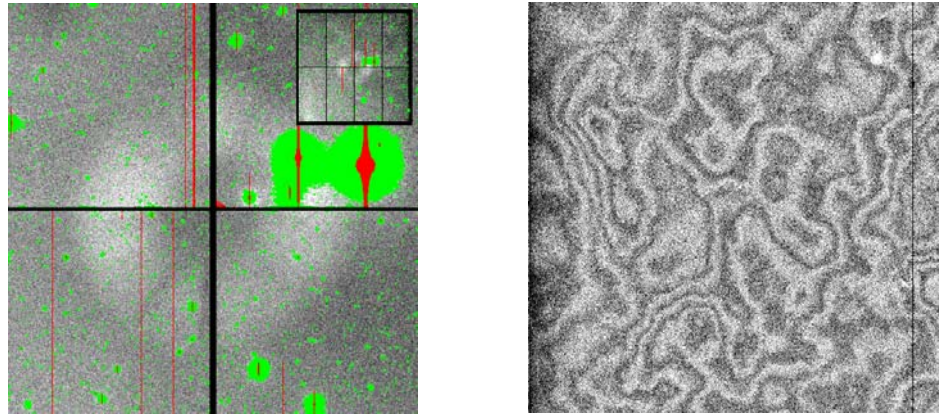


FIGURE 2.6: Example of the pupil ghost pattern (*left*, with bright targets and artifacts masked) near the intersection of the central 4 detectors, and the fringe pattern (*right*) in a 512 x 512 pixel region.

Flat-Field Correction

The flat-field correction removes the variations in the pixel-to-pixel response of the detector. Ideally the flat-field is derived for each filter from blank sky (i.e., the sum over all science images of the background regions), in order to match the illumination of the pixels in science images as well as the color of the background. However, if there is insufficient illumination of the background pixels it may not be possible to construct a sky flat of sufficient quality (see “Sky Delta-Flat” on page 2-26). In any case, the flat-field correction is performed by dividing each science frame by the flat-field templates for the corresponding filter: first by the dome flat, and then by the sky flat (if available).

World Coordinate System Calibration

The WCS calibration for science images is described by a two-dimensional polynomial (the function type and coefficients are found in the header) of a tangent-plane projection of stellar coordinates to the image pixel grid. The lower-order terms relate to the location of the reference pixel on the sky, the plate scale, and the rotation of the image, while the higher-order terms relate to non-linear effects of the optical system (such as image distortion) and differential atmospheric refraction. The form and order of the function varies with the filter and with the airmass of the observation. The initial values for all but the zero-point terms are taken from prior, full WCS solutions of calibration images where the astrometry of the stars in the field is known with very high accuracy; the initial value for the telescope pointing is taken from the TELRA and TELDEC header keywords, which are supplied by the telescope control system.

A full WCS solution is determined for each CCD by associating centroids of stars in the science images with objects in an astrometric catalog. Since the number of suitable stars in any given image (and their distribution within the image) can vary considerably, depending upon such details as the exposure time, ambient seeing, and clouds, the input list to the WCS solution includes roughly 100 additional pseudo-stars, which are merely computed points from the trial WCS solution. Thus, if the number of genuine stars in the image is small compared to the pseudo-stars, the high-order terms in the WCS solution will be dominated by the trial solution. If instead the number of genuine stars is large, they will dominate the WCS solution. In all cases, only the genuine stars contribute to determining the zero-point. The WCS solution, while robust, may fail if the telescope pointing is in error by several arcminutes or more (which is rare). See “Sources of Error” on page 2-27 for details.

Photometric Calibration

An estimate is made of the magnitude zero-point of each science image by comparing the instrumental magnitude of each field star to their published magnitudes in nearby passbands in a reference catalog, applying color transformations as necessary. Currently, the reference photometric catalog is USNO-B1.0 (see Monet, et al. 2003). Note that the result of the photometric calibration is to populate the science header with keywords—the pixel values remain unchanged, and have units of detected photons s^{-1} .

One quantity of use, the photometric depth of the exposure, is defined as:

$$-\frac{2.5}{2.3026} \log\left(\frac{3.988 \cdot DIQ \cdot \sigma}{\sqrt{A}}\right) + m_{zero}$$

In physical terms, the photometric depth is the faintest point-source that can result in an $5\text{-}\sigma$ detection above the sky background, in units of magnitudes. In the equation above, DIQ is the delivered image quality (expressed as the value of the header keyword `SEEING` in the image header) in units of arcseconds, σ is the noise in the background in ADU, A is the area of a pixel in arcsec^2 , and m_{zero} is the magnitude zero-point. This quantity is stored in the header of the calibrated images as the value of the `PHOTDPTH` keyword.

At present the photometric calibration is not adequate to support science, and is intended solely to provide a rough estimate of exposure depth to support queries from the Virtual Observatory. See “Sources of Error” on page 2-27 for details.



The magnitudes for the USNO-B1.0 catalog were for the most part derived from photographic source material and have high uncertainties. In addition, the mapping from filters used with the Mosaic cameras to USNO-B bandpasses, and then the color transformation from USNO-B to the SDSS filter set, introduces substantial (but uncharacterized) additional uncertainties. The resulting magnitude zero-point and photometric depth given in the headers of Mosaic science data are uncertain by an unknown amount that may approach 0.5 mag.

Image Re-projection

A single, re-projected Mosaic image is constructed by resampling, using a *sinc* interpolation, the component science image sections. This form of the science data product is easier to use for image stacking and inter-comparisons, without the need to handle the distortion mapping. The astrometric system is a tangent-plane projection with a uniform sampling of $0.25 \text{ arcsec pixel}^{-1}$, oriented with North “up” (i.e., Declination increases along Axis 2) and East “to the left” (i.e., Right Ascension decreases along Axis 1). The tangent point is selected from a grid on the sky with roughly 1° steps in RA, and exactly 1° in Dec. This selection makes it easy to stack images that are part of a sequence of small spatial dithers.

Image Stacking

The spatial footprint of images obtained during a single observing run using the same filter are compared, and those that have at least a 10% spatial overlap are combined into an image stack, which is an image containing the union of the spatial extent of all the constituent images. By construction, the pixel grids of the constituent images are aligned (see “Image Re-projection” above), so the first approximation to the output stack is the median of all non-masked pixels in the stack, after scaling to a common exposure time (if needed) and adjusting for the average sky background in each input image. This approximation is used to identify outliers in the constituent images (to eliminate cosmic rays and hot pixels), which are marked in the mask files. Ultimately the stack is constructed from the mean of the constituent images, after masking bad pixels, scaling by the exposure times, adjusting for the backgrounds, and weighting the input inversely by the seeing for each constituent image. The background level in the stack is the mean of the input image backgrounds, scaled by the exposure times.

2.3.2 Calibration Reference Files

The calibration reference files that are used in the pipeline processing are constructed for each observing run where a sufficient number of appropriate exposures exist. For all but the bias structure file, the exposures that are used for calibration are affected by multiple instrumental signatures. It is important to distinguish between the additive backgrounds and the multiplicative sensitivity variations in order to avoid biasing the photometric accuracy of the processed science frames. Thus, the path to creating the reference files is an iterative one, and involves isolating the various effects, storing a characterization of the effect in a template image, and using these templates to construct down-stream reference files.

The background includes two artificial sources: a pupil ghost, and a fringe pattern that is caused by the night sky emission lines. The nature of these effects and that of the flat-field was explained above; key properties of these effects are summarized in Table 2.7. Each effect differs somewhat in its spatial scale, amplitude, color dependence, and stability; these differences are in fact what makes it possible to separate out their respective contributions. Note that the background effects may not be apparent at all in some science images.

TABLE 2.7: Background Characteristics

Effect	Contribution	Spatial Scale (pix)	Amplitude	Color Dependence	Notes
Pupil Ghost	Additive	2300	10%	High ^a @blue & red	Spatially stable per filter; amplitude depends on field brightness.
Fringe Pattern	Additive	10 s to 100 s	1–10% of sky	Strong	Spatially stable per filter; amplitude variable in minutes to hours.
Flat-Field	Multiplicative	2	~1–2% ^b	Moderate	Stable spatially & temporally, apart from shadows of dust particles.

a. Effect is much smaller for Mosaic-2, where the corrector has a superior AR coating.

b. Localized variations of >10% are common near detector blemishes or dust particles.

With the exception of the bias and dome-flat images, all calibration reference files are generated from the bias- and cross-talk-corrected science frames themselves. Masks are then generated for each science frame that mark the locations of artifacts (e.g., bad columns, bleed trails, and cosmic rays) and astrophysical objects in the field. The masked science frames for each filter are then combined to yield master sky frames in order to characterize the background effects, as explained below.

Bias Structure

The master bias structure file is constructed very simply by applying the bias over-scan correction to each of several zero-second exposures, trimming the over-scan regions, and averaging the result (with rejection of outliers). Once constructed, both steps in the bias correction can be applied to all images.

Dome Flat-Field

Dome flats, or exposures of an illuminated screen affixed to the interior of the telescope enclosure, are used to form the first approximation to the true flat-field. The process for constructing the master dome flat is illustrated in Figure 2.7. After the bias correction is applied, the images for each filter are averaged (with rejection of outliers and masking of bad columns). The next step⁵ is to apply a template mask (from a library) with the same shape and spatial extent as the pupil ghost, so that a ratio may be determined between the portions of the dome flat-field image that are affected by the pupil ghost and those that are not. The ratio is applied to the pupil mask to generate a ghost template image that is divided out of the averaged dome flat-field image for each filter. This leaves the dome-flat template images, sans pupil ghost.

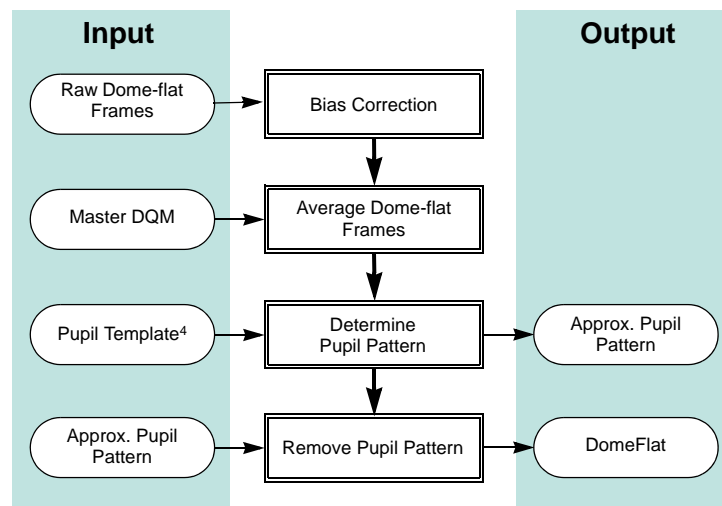


FIGURE 2.7: Process for characterizing the dome flat-field for each filter. Input dome-flat frames are uncalibrated. Pupil pattern characterization/removal applies to Mosaic-1 data obtained at the 4-m telescope only.

For some observing runs there are few if any dome-flat exposures. In this case, if there are exposures of the twilight sky (a.k.a., twilight-flat exposures) avail-

5. For Mosaic-1 data obtained at the 4-m telescope only.

able, these are processed in much the same way as described above and are used in place of the dome-flats.

Pupil Ghost

An accurate pupil ghost pattern is created⁶ for each affected filter from the science images themselves, as illustrated in Figure 2.8. The science images are first corrected for cross-talk and bias, before applying the dome flat. The non-masked portions of the images are averaged to produce a sky frame. The same pupil template mask mentioned above is used to create a much improved pupil template for each filter.

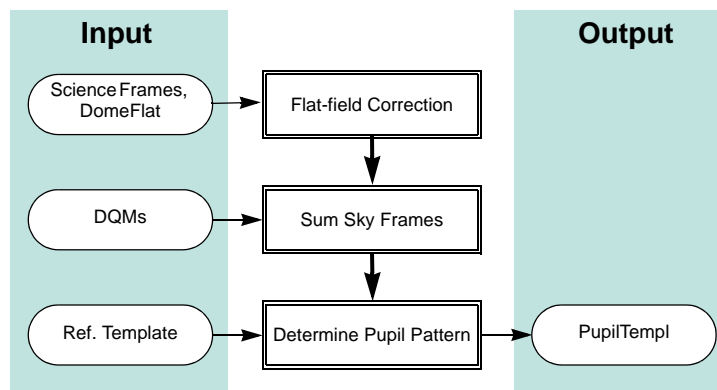


FIGURE 2.8: Process for characterizing pupil ghost pattern for each filter. Input science frames have had cross-talk and bias corrections applied.

Fringe Pattern

Having characterized the additive pupil ghost pattern, the science images are processed once again to scale and remove this pattern from each individual science image, and to correct the results by the dome flat. As illustrated in Figure 2.9, the frames are masked and combined, leaving a sky frame for each filter with the fringe pattern signature. This pattern can be characterized by smoothing the sky frame with a smooth, two-dimensional function with a width comparable to the fringe period, leaving a fringe template for each filter. Although in practice some or all of the fringe pattern within the pupil ghost template region is corrected by the pupil ghost pattern, this is not of concern because both terms are additive.

6. For Mosaic-1 data obtained at the 4-m telescope only.

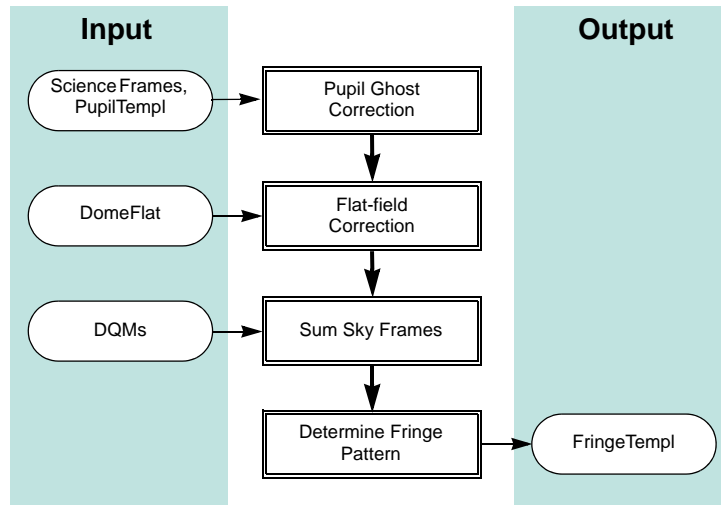


FIGURE 2.9: Process for characterizing the fringe pattern for each filter. Input science frames have had cross-talk and bias corrections applied.

Sky Delta-Flat

Once the pupil ghost and fringe pattern templates have been determined, an improvement to the flat-field can be generated from the accumulated night-sky background for each filter, provided there are enough counts. A flat-field generated in this way will be more closely matched to the science frames in the illumination pattern (i.e., large-scale, artificial gradients can be minimized), and in the color of the incident light (for which the effect is greatest for objects that are at or below the sky brightness). The processing of science data to determine the sky flat-field is shown in Figure 2.10. After correcting for cross-talk and bias, the pupil ghost and the fringe pattern are each scaled and subtracted from the science images, and the dome flat is applied. The results are masked and averaged to form a sky delta-flat template. The effect of applying this correction at full resolution is to use the sky as the flat-field, rather than the dome flats.

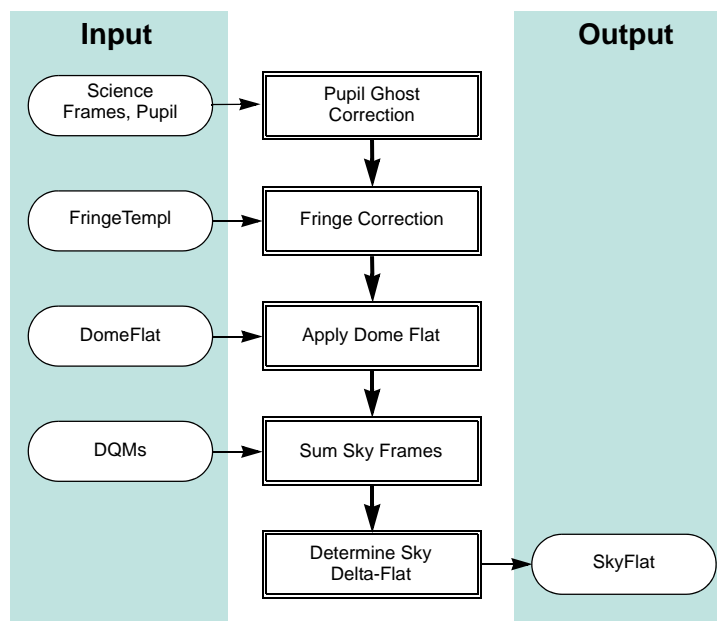


FIGURE 2.10: Process for characterizing the sky-flat for each filter. Input science frames have had cross-talk and bias corrections applied.

To be of sufficient quality, the sky flat-field must be composed of at least five (masked) input images, and have a signal-to-noise ratio of at least 50. If there are insufficient counts in the pixel-to-pixel sky delta-flat template, the sky delta-flat is smoothed by a function with a width of 255 pixels. In this case the dome-flat corrects for pixel-to-pixel variations in sensitivity, but the sky delta-flat corrects the dome-flat for low-order illumination effects.

2.4 SOURCES OF ERROR

This section describes the accuracy that can be expected for the major data products, the major sources of error, instrument foibles, and other noteworthy problems and issues with Mosaic data.

2.4.1 Astrometry

The astrometric accuracy for the image coordinate system is fundamentally limited by the accuracy of the astrometric catalog used to determine the WCS solution, which for the present is limited to USNO-B1.0. This catalog has the advantage of full-sky coverage, and a faint limiting magnitude that provides a

good overlap in the brightness range covered by most Mosaic exposures. Typical accuracies obtained for the WCS solution (0.25 arcsec measured in RMS deviations from the fit) are comparable to the accuracy of the catalog. The geometric stability of the Mosaic cameras is good, although rotations of the field of $\sim 1^\circ$ are common after the camera has been reinstalled for an observing block.

There are two known circumstances where the pipeline WCS solution may fail entirely. The first is if the trial WCS is missing entirely from the raw data header, which is rare. The second case is if the telescope pointing as recorded in the RA and DEC (or TELRA and TELDEC) keywords is too far from the actual pointing, in which case the WCS solution will not converge.

2.4.2 Photometry

The photometric stability of the Mosaic cameras is relatively good, and with care and good flat-fielding, it is possible to achieve photometric accuracies of 1%. However, **at present the photometric calibration provided by the pipeline processing is not adequate to support science** and is intended solely to provide a rough estimate of exposure depth to support queries from the Virtual Observatory. While the systematic uncertainty may be large, within a sequence of observations covering the same region of the sky, the relative uncertainties are significantly smaller and provide a useful diagnostic on the photometric stability of the sky.

The photometric performance for any given image depends mostly on a number of external factors, including the sky conditions and reflectivity of the telescope optics (both of which are time dependent). Representative photometric zero-points and color terms for some standard, broadband filters are given in Table 2.8 for the Mosaic-2 camera. The equations used to fit the standard star photometry are of the form:

$$u = U + A_0 + A_1X + A_2(U - B)$$

$$b = B + B_0 + B_1X + B_2(B - V)$$

$$v = V + C_0 + C_1X + C_2(B - V)$$

$$r = R + D_0 + D_1X + D_2(V - R)$$

$$i = I + E_0 + E_1X + E_2(V - I)$$

where capital letters are the standard magnitudes, lower-case letters are instrumental magnitudes ($25 - 2.5\log(ADU \cdot s^{-1})$), X is the airmass, and the first and last subscripted coefficients are given in the table.

TABLE 2.8: Representative Photometric Coefficients for Mosaic-2 Camera

Filt.	CCD 1	CCD 2	CCD 3	CCD 4	CCD 5	CCD 6	CCD 7	CCD 8
Zero-Point								
<i>U</i>	2.217±0.007	2.220±0.005	2.231±0.005	2.254±0.008	2.234±0.010	2.215±0.005	2.216±0.005	2.227±0.009
<i>B</i>	-0.107±0.008	-0.120±0.008	-0.115±0.008	-0.111±0.009	-0.111±0.008	-0.101±0.008	-0.106±0.008	-0.104±0.008
<i>V</i>	-0.448±0.008	-0.472±0.004	-0.472±0.004	-0.476±0.011	-0.475±0.004	-0.471±0.006	-0.472±0.005	-0.475±0.007
<i>R</i>	-0.636±0.004	-0.633±0.004	-0.648±0.004	-0.632±0.004	-0.628±0.004	-0.616±0.004	-0.629±0.005	-0.624±0.006
<i>I</i>	-0.089±0.010	-0.118±0.008	-0.076±0.010	-0.094±0.008	-0.094±0.004	-0.123±0.007	-0.113±0.011	-0.088±0.010
Color Term								
<i>U</i>	0.027±0.019	0.028±0.015	0.021±0.015	0.018±0.019	-0.025±0.024	0.019±0.016	0.015±0.016	-0.002±0.021
<i>B</i>	-0.069±0.010	-0.062±0.010	-0.058±0.010	-0.055±0.011	-0.056±0.010	-0.079±0.011	-0.081±0.010	-0.068±0.010
<i>V</i>	0.038±0.009	0.044±0.005	0.042±0.005	0.060±0.012	0.063±0.005	0.041±0.007	0.039±0.006	0.056±0.008
<i>R</i>	-0.025±0.008	-0.037±0.008	-0.022±0.008	-0.032±0.008	-0.028±0.008	-0.045±0.008	-0.035±0.010	-0.029±0.011
<i>I</i>	0.009±0.009	-0.002±0.007	-0.008±0.009	0.006±0.007	0.003±0.004	-0.002±0.006	0.003±0.011	0.011±0.010

2.4.3 Anomalies

Metadata

Critical metadata in raw science data files may sometimes be missing or have incorrect values. However, certain of the metadata in the headers of calibrated data, notably the WCS information and the filter name, are corrected during the course of pipeline processing (unless the calibration fails). Metadata *added* by the pipeline during processing are not in question.

Detector Performance

In September 2003, the CCD 3 in the Mosaic-2 camera failed, and was replaced in April 2004. Between these dates, the image extensions for this detector are still present in the data files, but contain no meaningful data.

The CCD array controllers for Mosaic-1 are known to suffer data drop-outs on occasion. The most recent documented cases occurred intermittently during January–May 2009, with array 2. This anomaly manifests itself in the data as a constant value everywhere in the affected array.

Bias Stability

It is possible to improve upon the bias correction by fitting the averaged over-scan vector with a polynomial (of order ~ 100). This approach would have the effect of smoothing the correction to reduce the effect of noise in the over-scan region. Unfortunately, the bias level is known on occasion to suddenly change (or jump) during read-out. This makes the line-by-line approach to the over-scan correction more robust.

Negative Saturated Pixels

Saturated pixels (where the accumulated charge exceeds the full-well, e.g., in the cores of over-exposed stars) will have negative values when the binning factor (given in the CCDSUM keyword) is 2×2 or higher.

2.5 REFERENCES & FURTHER INFORMATION

Contributing Authors

A large number of people have contributed to the technical knowledge of the Mosaic cameras. Extensive material has been contributed by George Jacoby (lead author of the first version of the Mosaic Instrument Manual), and by Heidi Schweiker and Buell Jannuzi (lead authors of Version 3 of the Instrument Manual). Other substantial contributors were: Taft Armandroff, Todd Boroson, Jim De Veny, Steve Heathcote, Tod Lauer, Bob Marshall, Phil Massey, Gary Muller, Knut Olsen, Rich Reed, Frank Valdes, David Vaughnn, and Dick Shaw. Documentation on the reduction of Mosaic data is also fairly extensive, much of which was authored (see below) by Frank Valdes (in IRAF documentation); Frank Valdes, Rob Swaters, and Tracy Huard (in pipeline documentation); and Heidi Schweiker, Buell Jannuzi, and Frank Valdes (in the form of the NDWFS data reduction notes).

References

Jacoby, G. H., Laing, M., Vaughnn, D., Reed, R., & Armandroff, T., 1998, *A New Wide-Field Corrector for the Kitt Peak Mayall 4-m Telescope*, SPIE 3355, 721

Jannuzi, B., Claver, J., & Valdes, F. 2003, *The NOAO Deep Wide-Field Survey Mosaic Data Reduction Notes* (Tucson: NOAO)⁷

7. Available at <http://www.noao.edu/noao/noaodeep/ReductionOpt/frames.html/>

- Massey, P., Armandroff, T., De Veny, J., Claver, C., Harmer, C., Jacoby, G., Schoening, W., & Silva, D. 2002, *Direct Imaging Manual for Kitt Peak* (Tucson: NOAO)
- Monet, et al. 2003, *AJ*, 125, 984
- Muller, G. P., Reed, R., Armandroff, T., Boroson, T., & Jacoby, G. 1998, *What is Better than an 8 K x 8 K Mosaic?*, *SPIE*, 3355, 487
- Schweiker, H., & Jannuzi, B. T. 2004, *NOAO CCD Mosaic Imager User Manual* (Version 3.0: Tucson: NOAO)
- Walsh, J. R., Pirzkal, N., & Pasquali, A. 2002, *Modelling the Fringing of the ACS CCD Detectors*, in 2002 *HST Calibration Workshop*, ed. S. Arribas, A. Koekemoer, & B. Whitmore (Baltimore: STScI)
- Wolfe, T., Reed, R., Blouke, M., Borson, T., Armandroff, T., & Jacoby, G. H. 1998, *CCD Detector Upgrade for NOAO's 8192 by 8192 MOSAIC*, *SPIE* 3355, 487

For Further Reading

A document repository⁸ for the Mosaic-1 camera is available on the Web. A general discussion of data reduction techniques for CCD mosaics was published by Frank Valdes, who also implemented these techniques in IRAF, including most of the applications that are used in the current Mosaic pipeline. Additional, more recent papers on the Mosaic pipeline appeared in the proceedings of the ADASS XVI conference.

Swaters, R. A. & Valdes, F. G., 2007, *The NOAO High-Performance Pipeline System: Mosaic Camera Pipeline*, in ASP Conf. Ser. 376, ed. R. A. Shaw, F. Hill, & D. J. Bell (San Francisco: ASP), 269

Valdes, F. G. 2002, *The Reduction of CCD Mosaic Data*,⁹ in *Automated Data Analysis in Astronomy*, ed. H. P. Singh, R. A. Gupta, & C. A. L. Bailer-Jones (New Delhi: Narosa Pub. House), 309

Valdes, F. G., & Swaters, R. A. 2007, *The NOAO High-Performance Pipeline System: Mosaic Camera Pipeline Algorithms*, in ASP Conf. Ser. 376, ed. R. A. Shaw, F. Hill, & D. J. Bell (San Francisco: ASP), 273

Various PI teams have used the Mosaic cameras to conduct major surveys. One team, lead by Phil Massey (Lowell Observatory), has published extensive

8. Mosaic-1 document repository: <http://www.noao.edu/kpno/mosaic/mosaic.html>

9. Available electronically at <http://iraf.noao.edu/projects/ccdmosaic/reductions/adaa/valdes2.pdf>

notes¹⁰ on their data reduction procedures. The following journal papers describe the calibration techniques and science results from this survey.

Massey, P., Olsen, K. A. G., Hodge, P. W., Strong, S. B., Jacoby, G. H., Schlingman, W., & Smith, R. C., 2006, AJ, 131, 2478

Massey, P., Olsen, K. A. G., Hodge, P. W., Jacoby, G. H., McNeill, R. T., Smith, R. C., & Strong, S. B. 2007, AJ, 133, 2393

10. Available at <http://www.lowell.edu/users/massey/lgsurvey/splog2.html>